Nuclear Instruments and Methods in Physics Research A 611 (2009) 52–68

Contents lists available at ScienceDirect

Nuclear Instruments and Methods in Physics Research A

journal homepage: www.elsevier.com/locate/nima

Radiation-induced point- and cluster-related defects with strong impact on damage properties of silicon detectors

Ioana Pintilie [a,*], Gunnar Lindstroem [b], Alexandra Junkes [b], Eckhart Fretwurst [b]

[a] National Institute of Materials Physics NIMP, Str. Atomistilor 105 bis, RO-77125 Bucharest, Romania
[b] Institute for Experimental Physics, University of Hamburg, Luruper Chaussee 149, 22761 Hamburg, Germany

ARTICLE INFO

Article history:
Received 7 July 2009
Received in revised form
1 September 2009
Accepted 8 September 2009
Available online 4 October 2009

Keywords:
Silicon detectors
EPI
FZ
MCz
Defect analysis
TSC measurements
N_{eff} predictions
S-LHC tracker

ABSTRACT

This work focuses on the investigation of radiation-induced defects responsible for the degradation of silicon detector performance. Comparative studies of the defects induced by irradiation with ^{60}Co-γ rays, 6 and 15 MeV electrons, 23 GeV protons and reactor neutrons revealed the existence of point defects and cluster-related centers having a strong impact on damage properties of Si diodes. The detailed relation between the "microscopic" reasons as based on defect analysis and their "macroscopic" consequences for detector performance is presented. In particular, it is shown that the changes in the Si device properties (depletion voltage and leakage current) after exposure to high levels of ^{60}Co-γ doses can be completely understood by the microscopically investigated formation of two point defects, a deep acceptor and a shallow donor, both depending strongly on the oxygen concentration in the silicon bulk. Specific for hadron irradiation are the annealing effects which decrease (increase) the originally observed damage effects as seen by the changes of the depletion voltage and these effects are known as "beneficial" and "reverse" annealing, respectively. A group of three cluster-related defects, revealed as deep hole traps, proved to be responsible specifically for the reverse annealing. Their formation is not affected by the oxygen content or silicon growth procedure suggesting that they are complexes of multi-vacancies located inside extended disordered regions.

1. Introduction

One of the most challenging applications for silicon detectors arises from their use in the inner tracking region of forthcoming colliding beam experiments as, e.g. Large Hadron Collider (LHC at the European research center CERN) and especially its planned upgrade (S-LHC), the International Linear Collider (ILC), or high-brilliance photon sources like the European XFEL foreseen also for the next decade [1–3]. Segmented silicon sensors (micro-strip and pixel devices) are at present the most precise electronic tracking detectors in high-energy physics experiments (HEP). This paper addresses the understanding of radiation damage effects resulting from the non-ionizing energy loss (NIEL) leading to displacement damage in the silicon bulk. Surface- and interface-related effects caused by ionization are on the other hand of considerable importance only for applications in environments with high X-ray doses (as e.g. in the European XFEL), a topic not addressed here.

For the S-LHC the detectors closest to the beam have to perform at hadron fluences up to several $10^{16}\,cm^{-2}$ under complex, long-term operation scenarios [4–6]. The limitations for their practical application in the hadron colliders are caused by irradiation-induced defects leading to changes in the effective doping concentration (N_{eff}) full depletion voltage (V_{dep}), the reverse current at the depletion voltage (I_{dep}) and the degradation in the charge collection efficiency (CCE) [5–14]. These device properties are subject to changes not only during irradiation but also during beam-off periods. Especially the long-term annealing effects in N_{eff} increase the initial depletion voltage and therefore they are of extreme importance envisioning extended operational periods of several years. In order to avoid a non-tolerable increase in the depletion voltage, the detectors have to be cooled not only during operation but also for the beam-off periods throughout the entire lifetime of the experiments. It would be of considerable importance if this cold storage could be avoided. One encouraging result for improving the radiation tolerance was obtained by the CERN-RD48 collaboration by performing an oxygen enrichment of float-zone (FZ) wafers used for detector fabrication. This defect engineering attempt was motivated by the assumption that a large O-concentration would inhibit the formation of the V_2O-defect thought to be the main reason for the observed change in the effective doping. A cost effective realization of oxygen enrichment up to several $10^{17}\,cm^{-3}$ was achieved by an in-diffusion of oxygen from the Si–SiO_2 interface (during treatments at high temperatures) after wafer oxidation. This procedure is called the DOFZ process (Diffusion Oxygenated Float Zone) and its main benefit is a considerable reduction in damage effects after

* Corresponding author. Tel.: +40 21 3690170.
E-mail address: ioana@infim.ro (I. Pintilie).

0168-9002/$ - see front matter © 2009 Elsevier B.V. All rights reserved.
doi:10.1016/j.nima.2009.09.065

gamma and charged hadron irradiation [15–18]. In contrast to charged hadron and γ-irradiation, neutron damage seems to be less dependent on the O-concentration. Although the obtained increase in the radiation tolerance may be sufficient to meet the requirements for LHC, the DOFZ process cannot be a solution for the much more demanding S-LHC application because of the intolerable increase in the depletion voltage up to more than 1000 V and the decrease in the charge collection efficiency (CCE) below the necessary threshold for the readout electronics. Therefore, further efforts for proper defect (and device) engineering leading to a radiation tolerance above the present level are indispensable.

Any promising attempt for radiation hardening of the material as well as improvements by modifying the detector processing will rely on a thorough knowledge of the generation of electrically active defects, which are responsible for the observed changes in the device properties at their operating temperature. This goal is addressed in our work focusing on a detailed investigation of specific radiation-induced defects (point- and cluster-related) and their direct correlation with device performance parameters. Pion-induced damage, dominating in the innermost layers of the tracking area, will result from both isolated point defects (mainly due to Coulomb interactions) and densely packed displacement regions (clusters) caused by energetic recoils from hadron reactions. A separation of both components can be best undertaken by studying damage caused by γ-irradiation (point defects) compared to neutron-induced damage (clustered displacements), while the mixture of both as envisioned in pion damage can be represented by studying the effects after high energetic proton irradiation. In addition several low-MeV electron irradiations proved to be useful for understanding the bridge between pure point defect-related and cluster-dominated defects.

2. Experimental details and techniques

Several kinds of n-type silicon material, presently discussed as candidates foreseen for use at S-LHC, have been investigated for this purpose:

Float-zone silicon FZ, produced by Wacker Siltronic [19], orientation ⟨111⟩, 300 μm thick, resistivity 3–4 kΩ cm, effective doping concentration $N_d \sim 10^{12}\,\mathrm{cm}^{-3}$. The standard processed p^+-n silicon diodes (labeled as STFZ) have an oxygen content of $[O] < 10^{16}\,\mathrm{cm}^{-3}$. O-enriched diodes (labeled as DOFZ) were obtained using an in-diffusion of oxygen from the $Si–SiO_2$ interface after wafer oxidation. The achieved O-concentration after a 72 h treatment at 1150 °C is $[O] \sim 10^{17}\,\mathrm{cm}^{-3}$ while the carbon concentration is at or below the detection limit (Fig. 1a).

Magnetic Czochralski silicon MCz, produced by Okmetic [20], orientation ⟨100⟩, 280 μm thick, resistivity 870 Ω cm, $N_d = 4.9 \times 10^{12}\,\mathrm{cm}^{-3}$. Due to the Czochralski process, this material has a high and almost homogeneous O-concentration around $[O] \sim 6 \times 10^{17}\,\mathrm{cm}^{-3}$ (see Fig. 1a).

Thin epitaxial silicon layers EPI, produced by ITME [21], orientation ⟨111⟩, 72 μm thick, resistivity 170 Ω cm, grown on 300-μm-thick highly Sb-doped Cz substrates. The effective doping concentration in EPI-diodes is $N_d \sim 2.5 \times 10^{13}\,\mathrm{cm}^{-3}$. In the present study both standard processed diodes (EPI-ST) as well as improved oxygen-enriched ones (EPI-DO) were used. For EPI-ST the oxygen is only partly out-diffusing from the O-rich Cz substrate during the epitaxial growth, thus leading to a quite inhomogeneous distribution (Fig. 1b). Measurements for EPI-ST, with 25, 50 and 75 μm thickness had been performed earlier, showing interesting effects on the average O-concentration [22]. For EPI-DO an additional diffusion step at 1100 °C for 24 h after wafer oxidation as part of the diode processing was included,

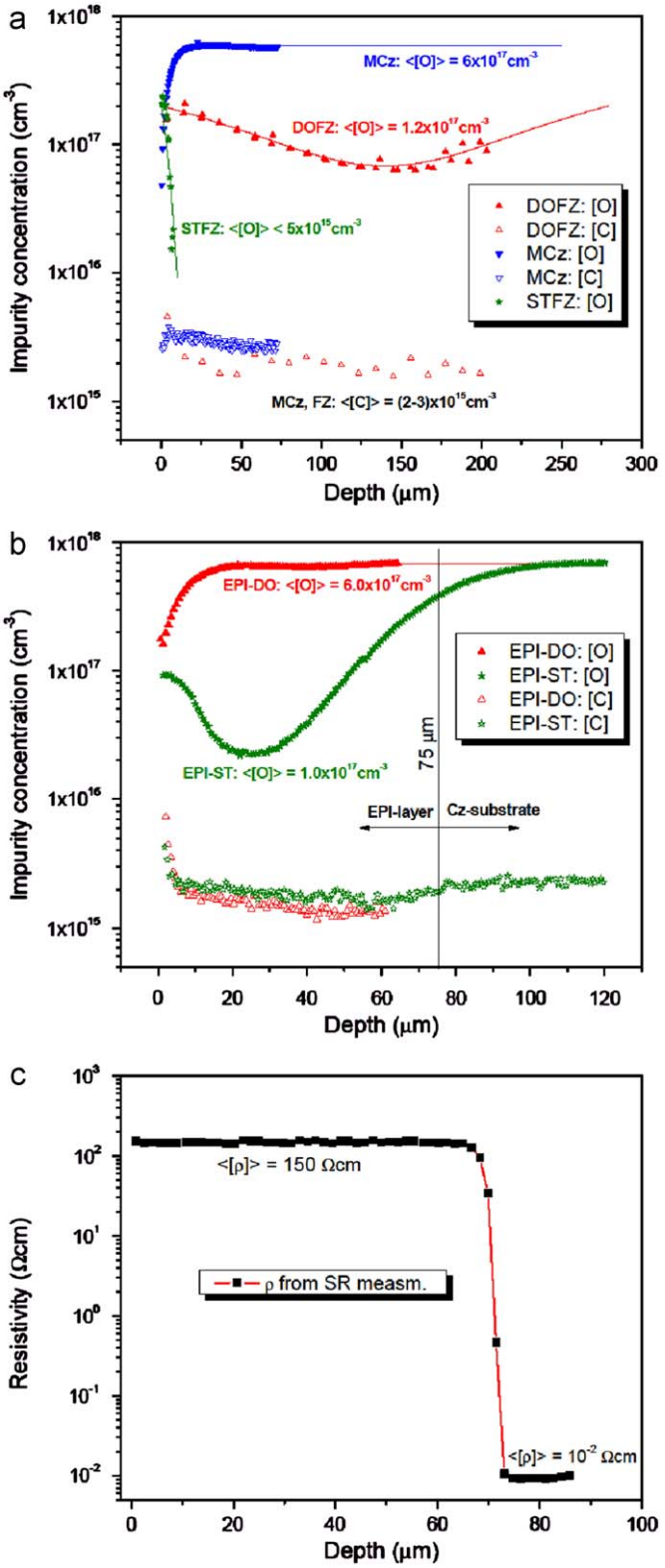

Fig. 1. (a) Depth profiles of oxygen and carbon concentrations measured with SIMS in MCz, STFZ and DOFZ diodes; (b) as (a) but in EPI-ST and EPI-DO diodes; (c) resistivity depth profile in a 75-μm-thick EPI diode resulting from spreading resistance measurements.

leading to a homogeneous O-distribution of $6 \times 10^{17}\,\mathrm{cm}^{-3}$, i.e. the same value as measured in the Cz substrate (Fig. 1b). The appreciable drop of [O] in about the first 10 μm is due to

out-diffusion through the front electrode is also present in the MCz sample (Fig. 1a).

In all cases diode manufacturing had been performed by the same company CiS [23], thus avoiding effects due to different process techniques. All diodes have a p^+ electrode of 25 mm^2 surrounded by a p^+ guard ring. The n^+ electrode area of 1 cm^2 is given by the geometrical dimension of the device. Oxygen and carbon concentration profiles in the diodes were measured by Secondary Ion Mass Spectroscopy (SIMS) at ITE [24] and are displayed in Figs. 1a and b. It should also be noted that for the EPI-diodes depth profiles of the resistivity had been performed using Spreading Resistance measurements (SR) on bevelled samples at ITME revealing a very homogeneous distribution throughout the epitaxial layer and an abrupt change at the EPI substrate interface [25] (Fig. 1c).

To distinguish between point- and cluster-related defects, damage effects have been investigated after irradiation with ^{60}Co-γ rays, producing only point defects, reactor neutrons for the study of predominant cluster damage and 23 GeV protons causing a mixture of clusters and isolated point defects. The γ-irradiations were done at the BNL ^{60}Co-γ source with dose values up to 5 MGy [26]; 6 and 15 MeV electrons were available at Stockholm [27]; the TRIGA reactor in Ljubljana was used for neutron irradiations [28] and the CERN-PS served for 23 GeV proton irradiation [29].

Neutron and 23 GeV proton fluences presented in this work are 1 MeV neutron-equivalent values [18], while for the electron irradiations the accumulated particle fluences are given. Further irradiation parameters which might have an impact on the results of the microscopic measurements and the macroscopic detector properties are the temperatures during irradiation and the exposure. The irradiation temperature was about 20 °C for the neutron irradiation and slightly above this value for all other exposures. On the other hand, the duration of exposure was quite different for the γ-ray and the particle irradiations. For the γ-irradiation the exposure time varied between 83 h and 35 days for the investigated dose range 500 kGy to 5 MGy. No annealing effects had been observed which indicates that the radiation-induced point defects are stable at room temperature. The exposure times for the different particle irradiations were much shorter, i.e. in the order of 10 to 60 min. For these cases, the situation is different because part of the damage leads to several cluster-related defects, which are not stable at room temperature. But the so-called short-term annealing time constants of some cluster-related defects, which have an impact on the reverse current (see Section 5), are in the order of 30 days at room temperature. Such time constants are long compared to the irradiation time and, therefore, will not lead to a considerable self-annealing effect during irradiation. Finally it should be mentioned that all samples were stored at temperatures below −20 °C after irradiation until the first measurements were performed.

The dependence of the defect generation on the radiation type is based on the following facts. The displacement energy in the silicon lattice, i.e. the minimum energy necessary to create a Frenkel pair (vacancy plus separated Si interstitial) is ~25 eV. The majority of effects expected after ^{60}Co-γ irradiation is due to Compton-electrons leading to a broad distribution of recoil energies for the primary knock-on Si-atoms (PKA) up to 140 eV, i.e. below the threshold energy for cluster generation, considered to be 5 keV [30]. Taking recombination effects for close pairs into account, it is therefore very unlikely to directly create larger complexes than a double vacancy. In contrast to this, Si-displacements by neutron interaction are dominated by head-on collisions, and, e.g. for 1 MeV neutrons the mean energy transfer to the Si atom is ~50 keV (note that the NIEL weighted mean energy of the Ljubljana reactor neutron spectrum is 1.7 MeV). The track length of a 50 keV PKA is about 100 nm with an extremely high density of displacements (cluster formation) [31]. On the other hand energy loss of charged hadrons is widely governed by Coulomb interactions with a PKA spectrum extending from dominant low energies (point defects) to quite large ones with a high probability of producing defect clusters [18,32]. Finally in the case of electron irradiation the maximum PKA energy for 6 MeV electrons is 18 keV (700 displacements!) and for 15 MeV it is 250 keV and hence even the average energy transfer would already approach the value encountered for 1 MeV neutrons (see above).

The "macroscopic" device performance of the investigated diodes was measured by means of capacitance–voltage (C–V) and current–voltage (I–V) diode characteristics. The radiation-induced changes in the effective doping concentration (N_{eff}), and full depletion voltage (V_{dep}) were determined from, respectively, C–V measurements performed using a frequency of 10 kHz and guard ring grounded. The most sensitive technique for analysis of electrically active defects is the Capacitance-Deep Level Transient Spectroscopy (DLTS). However, this method can be applied only for investigation of defects with low concentration, thus limiting the irradiation fluence to less than 10^{12} cm^{-2} and with the γ-dose below a few 10 kGy (depending on the doping concentration of the material). For this situation, apart from the damage-related current increase no change in the detector performance is seen and thus, the defect levels responsible for the deterioration after high-irradiation levels cannot be identified and correlated with the "macroscopic" characteristics of the detectors (N_{eff}, CCE). On the other hand, the reverse current increase is much more sensitive already at small fluence levels and thus cluster-related effects as they are expected to be relevant for the damage-induced generation current as measured at depletion voltage ($I(V_{dep})$), may be very well studied in parallel to DLTS measurements.

Therefore, for larger irradiation fluences (between 10^{12} and 10^{15} cm^{-2}) we have used the Thermally Stimulated Current method (TSC) [33,34]. It detects the centers, which trap free carriers in the material and allow us to determine the trapping parameters of defect levels needed to calculate their impact on the electrical properties of the device: activation energy, capture cross-sections for electrons and holes, defect concentration. The TSC experimental procedure consists of cooling the sample down to a low temperature where filling of the traps is performed (by illumination or forward biasing of the diode). The TSC current measurements are then performed during heating up (with a constant heating rate of 11 K/min) under reverse bias applied to the sample. If the reverse bias is high enough to maintain full depletion of the diode during the temperature scan, the active volume of the sample is well known (defined by the guard ring-controlled electrode area) and thus the defect concentrations can be calculated from the total charge released from the defects during the heating (peaks showing up in the TSC spectra).

3. Defect properties and detector performance

Many electrically active defects, induced by irradiation, are detected by DLTS and TSC experiments. Most of them (VO, V_2, C_i, C_iO_i, C_iC_s, IO_2) were already investigated in detail and no correlation with the "macroscopic" behavior of the diodes could be established [35–46]. The main characteristics of defects, from the electrical point of view, are the emission rates of carriers in the conduction and valence bands given by

$$e_{n,p}(T) = c_{n,p}(T) N_{C,V}(T) \exp\left(\pm \frac{E_T(T) - E_{C,V}}{k_b T} \right) \text{ with } c_{n,p}(T) = \sigma_{n,p}(T) \nu_{th,n,p}(T) \quad (1)$$

where $N_{C,V}$=effective density of states in the conduction/valence band, $E_{C,V}$=band edge energies, $E_T(T)$=energy of the defect level,

$\sigma_{n,p}$=electron/hole capture cross-section and $v_{th,n,p}$ is the average thermal velocity of electrons/holes.

The important features of a defect are: the capture cross-sections $\sigma_{n,p}$, the defect level position in the band gap E_T, the defect concentration N_T and the type of the defect (acceptor or donor like). Once these characteristics are known, the influence of a defect on the space charge density as well as on the leakage current can be calculated. The contribution to N_{eff} is given by the steady-state occupancy of the defect levels n_T that can be calculated according to the following relations resulting from the Shockley–Read–Hall statistics [34,47]:

$$n_T^{acceptor}(T) = N_T \frac{c_n n + e_p}{e_n(T) + e_p(T) + c_n(T)n + c_p(T)p}$$
$$n_T^{donor}(T) = N_T \frac{c_p p + e_n}{e_n(T) + e_p(T) + c_n(T)n + c_p(T)p}$$
$$N_{eff} = \sum n_T^{donor} - \sum n_T^{acceptor} \quad (2)$$

where n, and p, respectively, are the concentration of free electron holes in the space charge region (SCR), which can be neglected in diodes with low reverse currents.

The defect contribution to the reverse current at full depletion $I(V_{dep})$ is given by [47,48]

$$I(V_{dep})(T) = q_0 A d\left(\sum e_n(T) n_T^{acceptor}(T) + \sum e_p(T) n_T^{donor}(T)\right) \quad (3)$$

where q_0 is the elementary charge, A and d are the area and the thickness of the diode, respectively.

The donors in the upper part of the gap are traps for electrons, show the Poole–Frenkel effect (a certain dependence of the emission rate of electrons on the electric field) [49] and contribute with positive space charge to N_{eff} at room temperature (RT). The donors in the lower part of the gap are traps for holes, show no Poole–Frenkel effect and do not contribute to N_{eff} at RT unless they are close to mid-gap. In contrast, acceptors in the upper part of the gap, although they are traps for electrons, do not show the Poole–Frenkel effect, and can contribute to N_{eff} with negative space charge at RT only if they have close to mid-gap levels. The acceptors in the lower part of the gap are traps for holes, show the Poole–Frenkel effect and contribute with negative space charge to N_{eff} at RT. The most effective centers in generating leakage current are those having close to mid-gap levels, independent of their type (acceptor or donor like).

4. Point defects, predominantly after γ-irradiation

Knowing the already huge efforts spent on investigating defects after hadron irradiation, with no real success in finding the defects responsible for the detector deterioration, we have decided to start our investigations with the simplest case, i.e. in situations where only point defects are generated. This was achieved by performing irradiation with ^{60}Co-γ rays.

The diodes used for these investigations were processed on high-resistivity silicon oxygen lean (STFZ) and oxygenated (DOFZ) material (see Section 2). A very pronounced beneficial effect of the oxygen content on both the current and the depletion voltage was observed [8]. While the STFZ samples undergo a space charge sign inversion-SCSI (changing the space charge sign from initially positive in n-type silicon to negative, i.e. effectively p-type material), the oxygenated diodes did not show this effect but in contrast, showed a gain in the positive space charge with increase in irradiation dose. These "macroscopic" characteristics suggest the presence of both, a deep acceptor like defect, generated mainly in oxygen lean material, responsible for the SCSI effect and the high leakage current in STFZ material and a shallow donor in the upper part of the gap, generated mainly in oxygen-rich material, which causes the gain in the positive space charge with increase in irradiation dose. Detailed studies of electrically active defects by means of the TSC technique revealed indeed the generation of such point defects in the two types of materials. Examples of the many experimental results are given in the following.

4.1. Deep acceptor I_p

The I_p center is a point defect formed via a second-order process that is responsible for the observed type inversion effect in oxygen lean material after γ-irradiation [48,50, and 51]. It was detected so far in three charge states (−, 0 and +), with two levels in the band gap, a donor level in the lower part (E_V+0.23 eV) and an acceptor level at the middle of the gap (E_C–0.55 eV). This center is stable up to temperatures of 325 °C [52]. The corresponding TSC peaks are shown in Fig. 2a. The quadratic dose dependence (second-order generation) of the I_p center was previously found both for the STFZ and DOFZ diodes up to irradiation doses 2.80 MGy [48,50,51] and is displayed in Fig. 2b up to 5 MGy.

The present TSC investigations, extended up to 5 MGy, indicate a saturation tendency for the I_p center at about 2×10^{12} cm^{-3} (STFZ curves in Fig. 2b). The defect structure is still under debate. Due to its generation via a second-order process during irradiation at ambient temperature (when mainly single vacancies and interstitials are mobile) it was suggested that the best candidate is long searched for defect complex V_2O. The V_2O is the only one defect generated by a second-order process that was evidenced by Electron Paramagnetic Resonance [53,54] as a direct result of irradiation. On the other hand, there are studies based on the annealing of V_2 at high temperatures of diodes irradiated with small dose values that revealed the transformation of V_2 into another defect X in oxygen-rich silicon [55,56]. In these publications the X defect was associated also with the V_2O complex. However, the energy levels of the X and the I_p are very different and both cannot be attributed to the same defect. Contrary to the I_p center no influence of the X defect on the detector performance was observed.

4.2. Shallow donor BD

The BD center is a bistable donor (point defect) strongly generated in oxygen-rich material [48,57]. This center and its bistability have been first observed after ^{60}Co-γ irradiation in high-resistivity DOFZ material. In this case only for one of the defect configurations a clear TSC peak was recorded (see BD_A in Fig. 3a). The other configuration was suggested by the appearance of a large TSC signal in the low-temperature range (not shown here). One of the configurations is more stable if the material is exposed to day light (BD_B) while the other configuration (BD_A) starts to appear when the material is kept some time in the dark at RT (see Fig. 3a). The needed storage at RT in the dark to get the full transformation from BD_B to BD_A is decreasing with increase in irradiation dose suggesting that, similar to the earlier thermal donors in silicon, the defect configuration depends on the position of the Fermi level. The BD center has a linear dose dependence, indicating that it is generated via a first-order process (see Fig. 3b).

A clear evidence for the existence of the two configurations of this defect was obtained in medium-doped epitaxial layers irradiated with neutrons [57]. As can be observed in Fig. 4a, two clear TSC peaks associated with the two defect configurations could be detected. The TSC peaks recorded for different bias voltages have shown that for both defect configurations the emission rate of electrons increases with the electric field. This

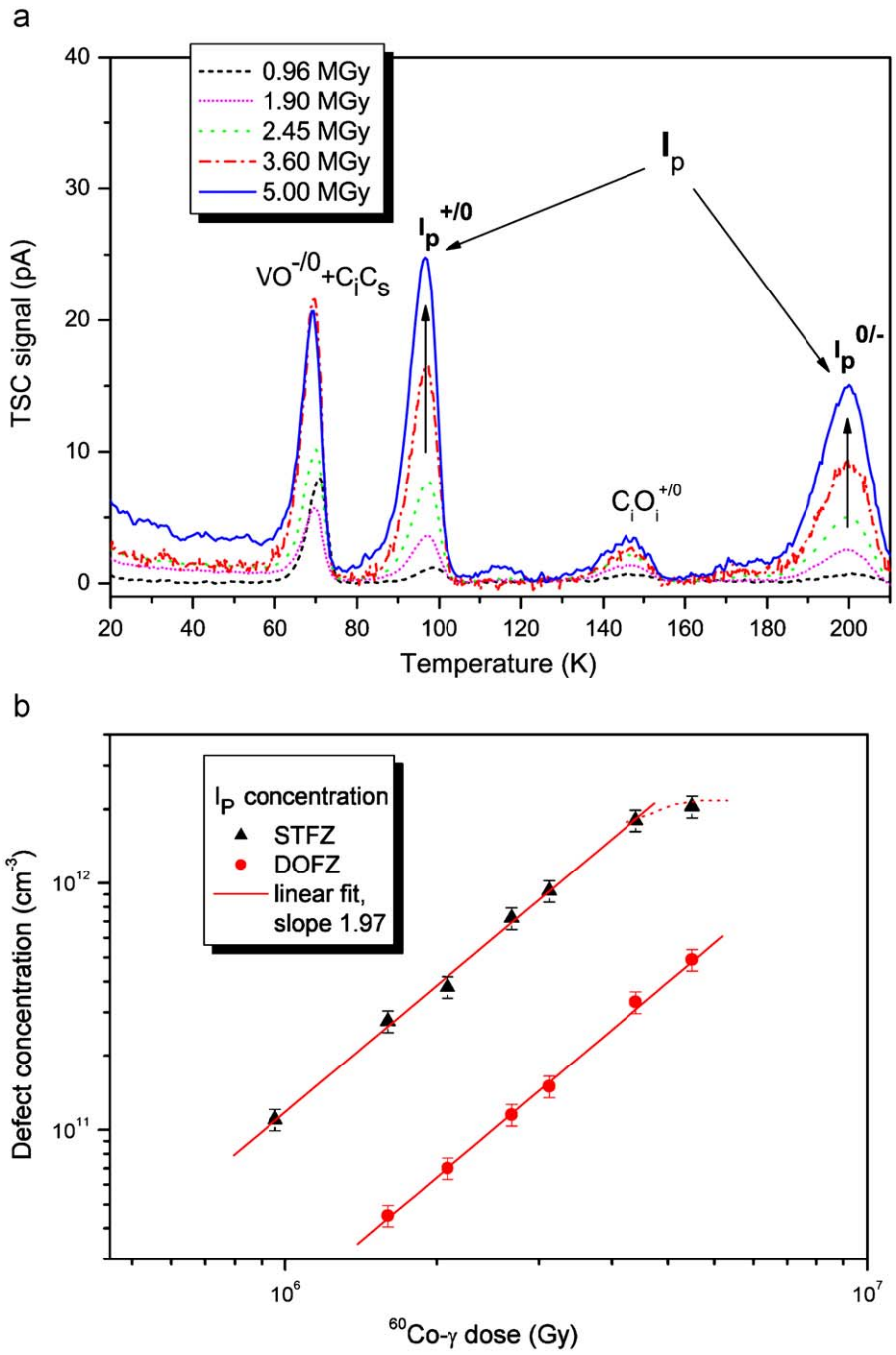

Fig. 2. (a) TSC spectra recorded on STFZ diodes after γ-doses between 0.96 and 5 MGy; (b) γ-dose dependence of the I_p defect concentration. Note: saturation tendency seen for STFZ at 5 MGy, slope in log–log scale presentation: 2.0, i.e. quadratic dose dependence.

effect is clearly observed in Figs. 4b and c where the TSC peak positions are shifting toward lower temperatures when increasing the applied reverse bias while their integrals are increasing. The analysis of the corresponding TSC peaks revealed that the field-enhanced emission rate is due to the Poole–Frenkel effect for both defect configurations, thus indicating that the defect is a donor in the upper part of the gap. Details about the analysis of TSC signals in the case of Coulomb centers (three-dimensional Poole–Frenkel effect) accounting for the spatial distribution of the electric field inside the samples can be found in [58], the zero field activation enthalpy was determined $\Delta H_a = E_C - 0.15$ eV for the BD_B configuration (transition between + and ++ charge states) and $\Delta H_a = E_C - 0.24$ eV for BD_A (transition between 0 and ++ charge states). Except for the oxygen lean STFZ material, the BD is detected in all other materials, independent of the type of irradiation. As a point defect it is strongly generated after γ-irradiation but is detected also after neutron and proton damage [34].

The bistability, donor activity and energy levels associate the BD center with the earlier thermal double donors TDD2 in Si [59–61]. These species of thermal donors can exist in two different structural configurations: one associated with the common shallow double donor state (TDD) with occupancy levels (0/+) and (+/++) at $E_C - 0.07$ and $E_C - 0.15$ eV, respectively, and a second configuration that form an Anderson negative U system [62] with a single occupancy level (0/++) at $E_C - 0.22$ eV.

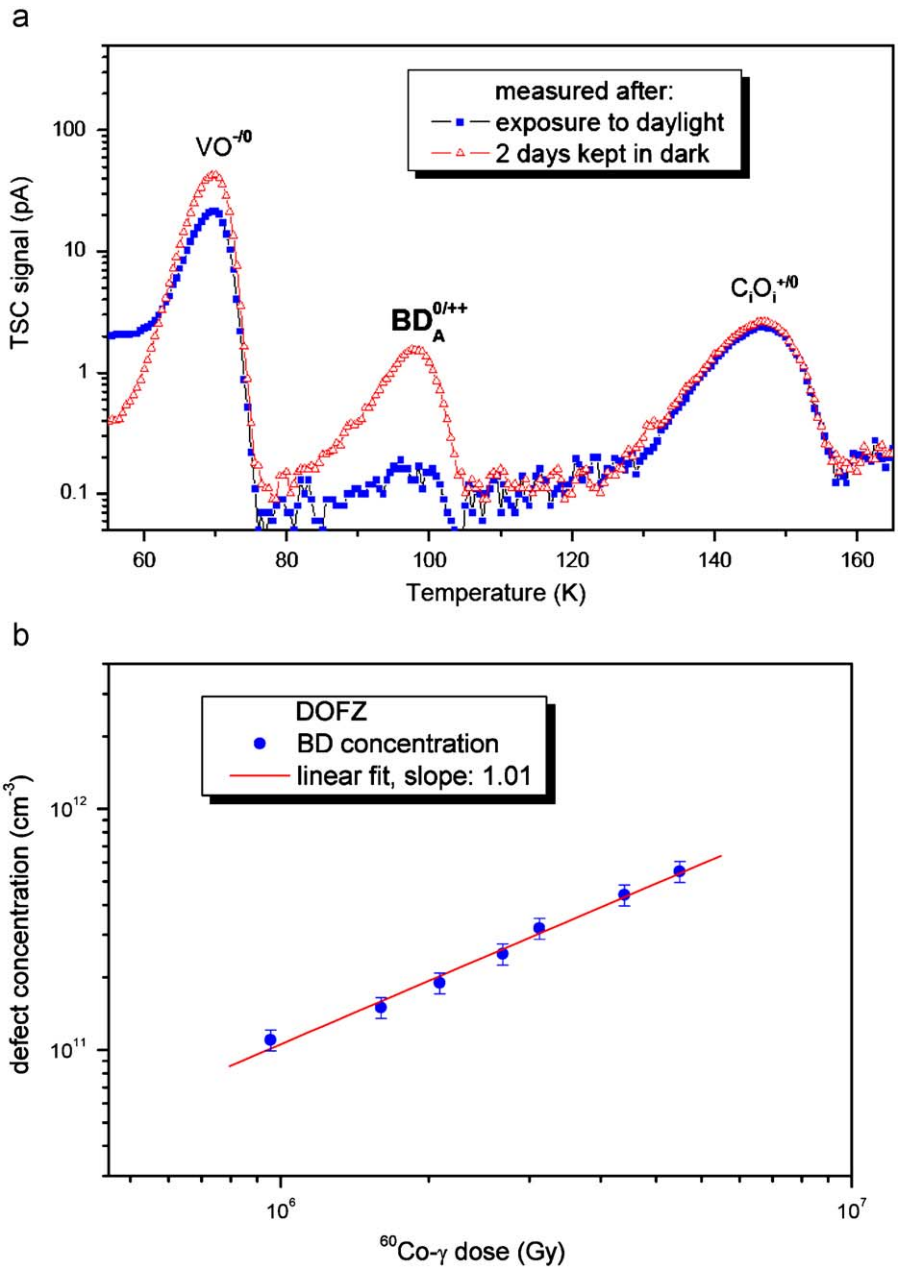

Fig. 3. (a) TSC spectra corresponding to forward injection of 2 mA for 30 s at 20 K recorded on DOFZ diodes after exposure to day light and after keeping the diode in the dark at RT for 2 days; (b) γ-dose dependence of the BD defect concentration. Slope in log–log scale presentation: 1.0, i.e. linear dose dependence.

4.3. *Predictions from the defect analysis for N_{eff} and I_{dep}*

Both centers, i.e. the I_p as well as the BD, have a direct influence on the effective doping concentration. The I_p center contributes with negative space charge while the BD center introduces a positive space charge. The contribution of these two centers to N_{eff} has been calculated according to Eq. (2) and the results are presented in Fig. 5a together with the values extracted from *C–V* measurements performed at RT. There is an excellent agreement between measured and calculated values for both STFZ and DOFZ devices. In the case of oxygenated material (DOFZ), the BD-defect concentration overcompensates the negative space charge introduced by the I_p center leading to the observed slight increase in the effective doping concentration (Fig. 5a).

Due to its mid-gap acceptor level the I_p center contributes significantly also to the reverse current at RT. The values of $I(V_{dep})$, calculated according to Eq. (3), by considering only the I_p center, are shown in Fig. 5b together with the values extracted from *I–V* measurements performed at RT. Also in this case the predictions deduced from the microscopic measurements represent the macroscopic findings fairly well. Especially the considerably lower leakage current in DOFZ is nicely reproduced and can therefore be attributed to the suppression of the I_p center due to the large O-concentration.

These results represent the first breakthrough in understanding of macroscopic deterioration effects on the basis of a detailed defect analysis and demonstrate that the beneficial oxygen effect in FZ silicon after electromagnetic irradiation results not only in the suppression of deep acceptors (as predicted by the defect models considering the formation of the defect complex V_2O [63]) but also in the creation of a bistable donor similar to the earlier stage thermal double donors TDD2 in oxygen-rich silicon. These donors can even over-compensate the negative space charge introduced by deep acceptors (I_p) such that no type inversion

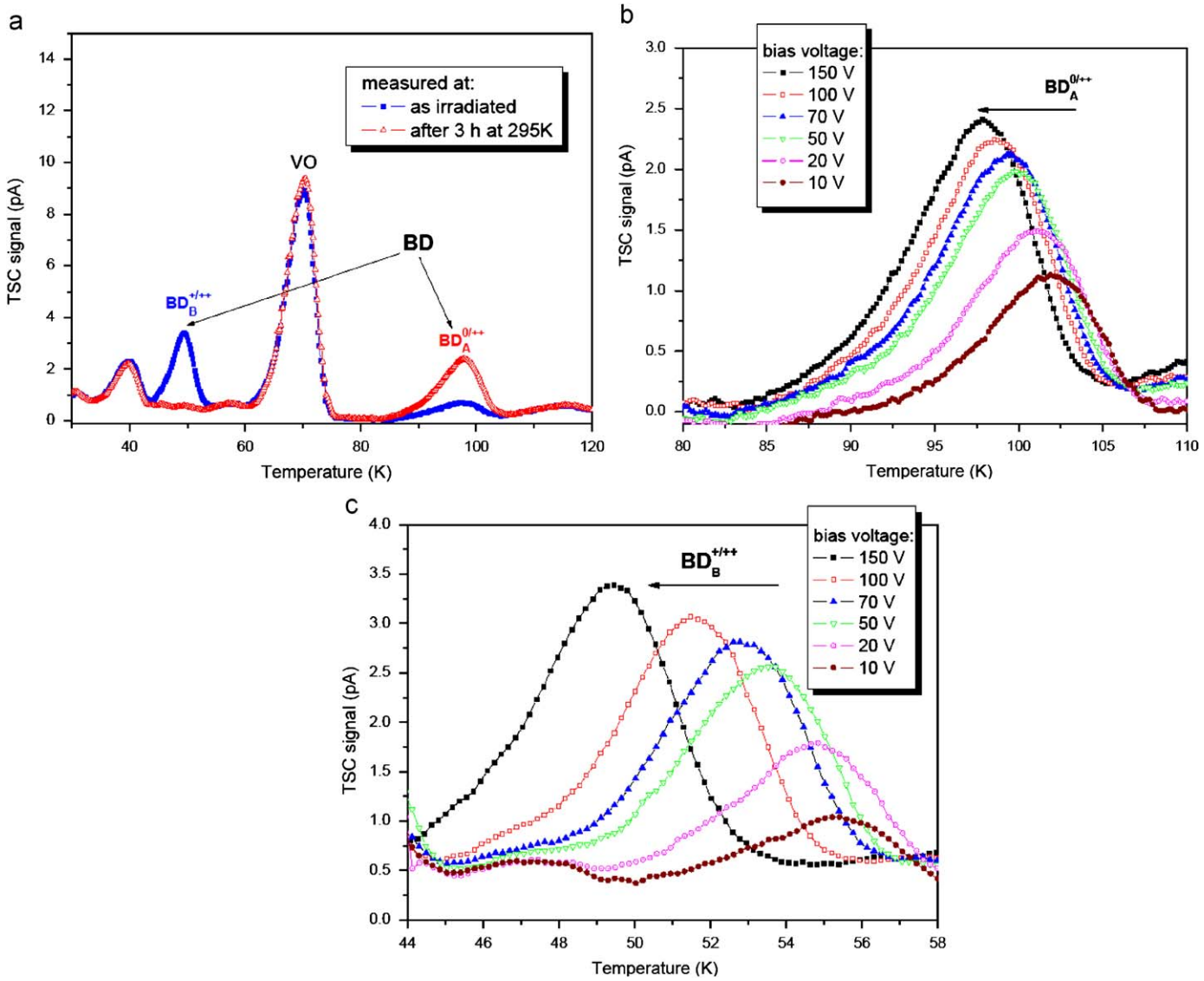

Fig. 4. Measurements on EPI-DO diodes after neutron irradiation with $\Phi_{eq}=5\times10^{13}\,cm^{-2}$. (a) TSC spectra corresponding to forward injection of 2 mA for 30 s at 5 K, recorded after exposure to day light and after keeping the diode in dark at RT for 3 h; (b) Poole–Frenkel shift of the TSC peak corresponding to the BD_A configuration; (c) Shift of the TSC peak corresponding to the BD_B configuration.

appears in DOFZ material even after very high dose values. Although no identification of the TDD2 was accomplished so far, it is well accepted that the oxygen dimers (O_{2d}) are part of the defect structure [64].

5. Defect studies after hadron irradiation

Contrary to low energetic particles, primarily electrons as secondary particles after γ-irradiation (photo- and Compton-effect), producing mainly point defects, more energetic particles, especially hadrons (pions, protons, neutrons or heavy ions) and to some extent also larger energy electrons (see Section 6) may lead to a cascade of many successive displacements, resulting in the formation of a large diversity of extended defects as densely packed conglomerates ("clusters") of vacancies and interstitials. The present knowledge on defect clustering is however very limited. Only recently some clear evidences for the formation of electrically active extended defects were reported [58,65,66]. Irradiation experiments with reactor neutrons and 23 GeV protons have revealed that there is a group of cluster-related defects with direct impact on the device characteristics at operating temperature. In addition a donor, not generated after γ-irradiation, is found here, and it is visible at moderate energy electron irradiations (see Section 6). These defects are discussed below. For this investigation 72 μm EPI-DO and EPI-ST as well as 280 μm MCz diodes had been used and annealing studies were performed at 80 °C.

5.1. Deep acceptors

The $H(116\,K)$, $H(140\,K)$ and $H(152\,K)$ centers, as already detected earlier [58], are traps for holes with acceptor type levels in the lower part of the band gap that show the Poole–Frenkel effect. As Coulomb centers, their emission rates depend on the local electric field. The parameters for the zero field emission rates reported in Ref. [58] are: $\sigma_p^{116\,K}=4\times10^{-14}\,cm^2$ and $\Delta H_a^{116\,K}=0.33\,eV$, $\sigma_p^{140\,K}=2.5\times10^{-15}\,cm^2$ and $\Delta H_a^{140\,K}=0.36\,eV$, and $\sigma_p^{152\,K}=2.3\times10^{-14}\,cm^2$ and $\Delta H_a^{152\,K}=0.42\,eV$.

These centers were first detected after irradiation with 1 MeV equivalent reactor neutrons by means of the TSC technique (see Fig. 6a) but are not seen after γ-irradiation, a strong indication

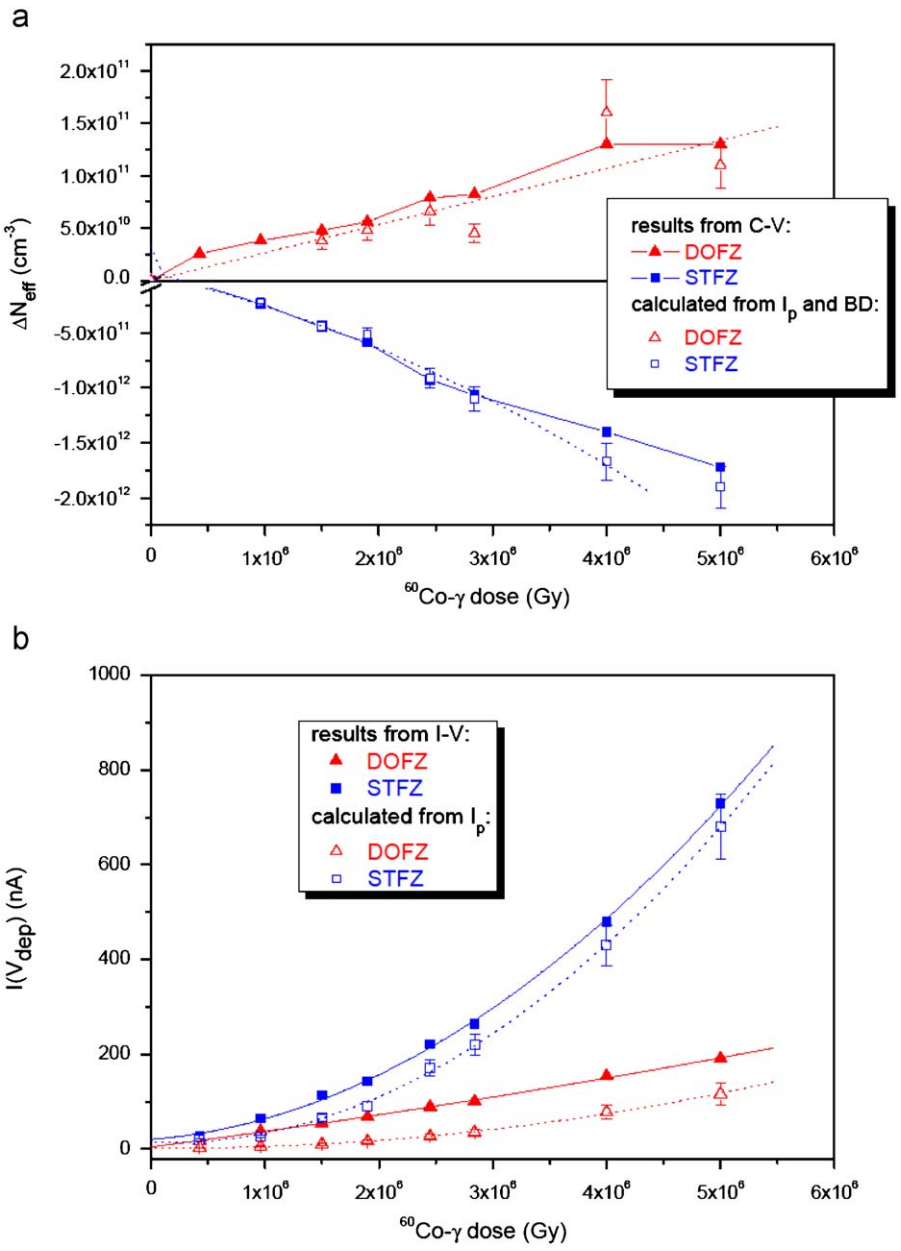

Fig. 5. Calculated and measured dose dependences: (a) For the irradiation-induced effective space charge concentration; (b) for the reverse current at full depletion, both for STFZ and DOFZ diodes.

that they are cluster related. We have also detected them after irradiation with 23 GeV protons and the results of TSC investigations are shown in Fig. 6b. As to be seen the defect concentrations are increasing with annealing time. As the defect levels are located in the lower part of the gap, they contribute fully with negative space charge to N_{eff} and are responsible for the long-term annealing (so-called "reverse annealing", see below). Results after an isochronal annealing stage of 300 °C clearly demonstrate the mentioned Poole–Frenkel shift for these hole traps and in addition a H(125 K) defect (Fig. 7a). Here it is also demonstrated that the I_p defect does not play a significant role after hadron irradiation.

5.2. Shallow donors

The E(30 K) defect, also clearly identified in Figs. 6a and b, is acting as a trap for electrons. Also this defect was only detected after hadron irradiation (and to some extent after energetic electron irradiation), but not after γ-irradiation. However contrary to the deep hole traps discussed above its generation rate after proton irradiation is at least a factor 6 larger than for neutron damage (compare Figs. 6a and b). As for the hole traps discussed above, the E(30 K) defect is generated mainly after irradiation, during the first 20 min at 80 °C, a finding subject to further investigation. The enhanced generation after proton irradiation suggests it to be an isolated "point defect" produced via the abundant low energy transfers after Coulomb interaction (further discussion in Section 6). The TSC investigations have shown that E(30 K) is a defect with enhanced field emission described by the Poole–Frenkel effect, as best seen after proton irradiation (see Fig. 7b) thus evidencing that it has a donor level in the upper part of the gap [67,68]. The parameters for the zero field emission rate describing the experimental results are: $\sigma_n^{30\,K}=2.3\times10^{-14}\,cm^2$ and $\Delta H_a^{30\,K}=E_C-0.1$ eV from the conduction band. This center contributes in its full concentration with positive space charge to

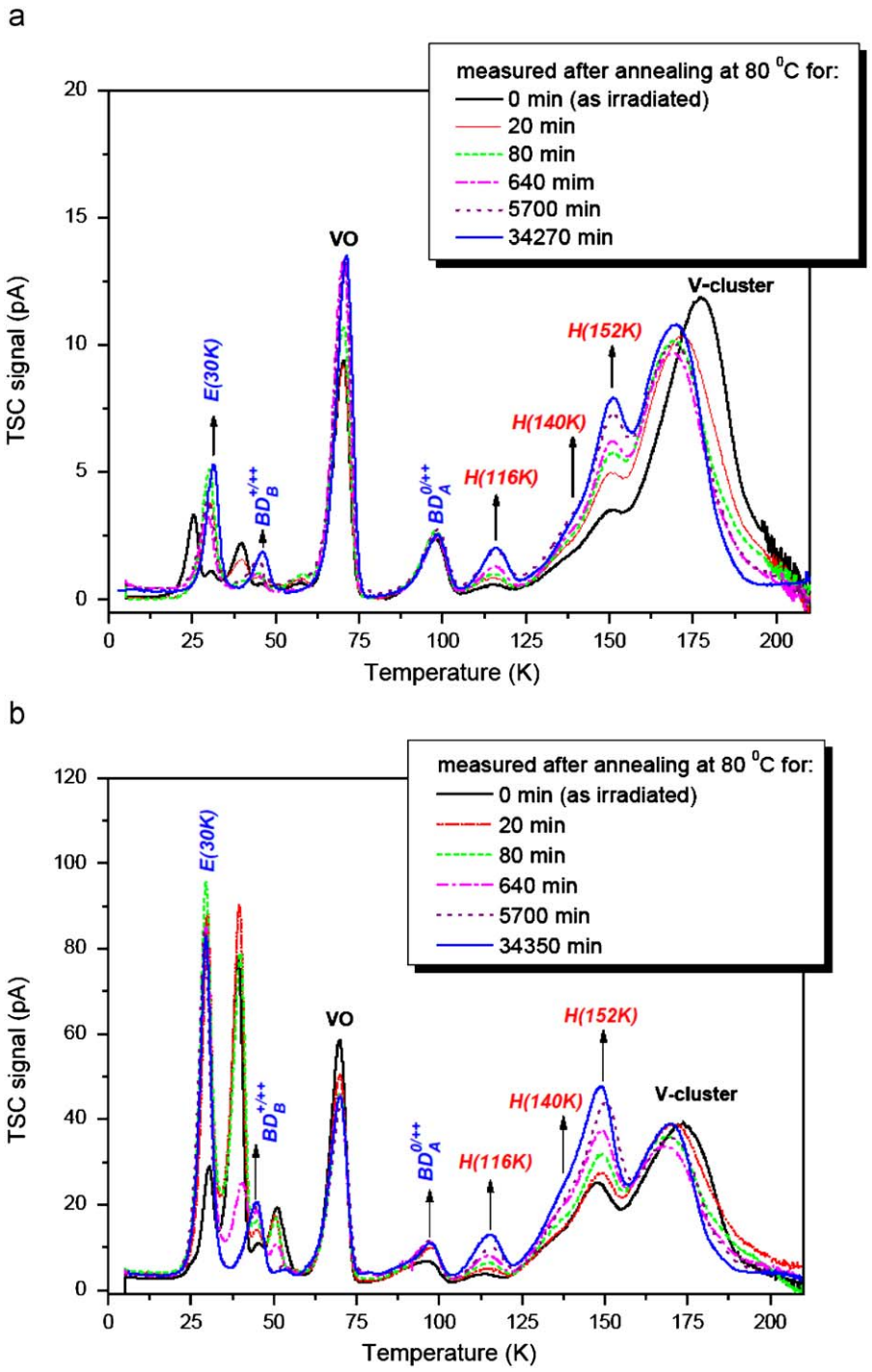

Fig. 6. (a) TSC spectra recorded on EPI-DO diodes after neutron irradiation with $\Phi_{eq}=5\times10^{13}\,cm^{-2}$ after different annealing times at 80 °C, measurements after forward injection of 2 mA for 30 s at 5 K; (b) same as in (a) but after 23 GeV proton irradiation with $\Phi_{eq}=2.3\times10^{14}\,cm^{-2}$.

N_{eff} and may be consequently partly responsible for the so-called "beneficial annealing" effect.

5.3. Material dependence

A comparison of TSC spectra obtained in EPI-ST, EPI-DO and MCz diodes after the same neutron irradiation of $5\times10^{13}\,cm^{-2}$ is displayed in Fig. 8 as example for long-term annealing at 80 °C. The different thicknesses of the MCz diode (280 μm) and the EPI ones (72 μm) have been taken into account for proper normalisation. One can clearly see that, while the overall H center concentration is about the same for all different materials with a slight enhancement of the $H(140\,K)$ in MCz, the BD_A formation is much larger in the EPI-DO than in the EPI-ST diode. For MCz we have only a considerably smaller BD component, an effect which had been observed before and may be due to the comparatively larger O-dimer concentration in EPI-diodes resulting from the growth process [34].

5.4. Comparison between "microscopic" predictions and "macroscopic" results

The results from the TSC defect investigations were used to predict the annealing effects of N_{eff}, which are then compared

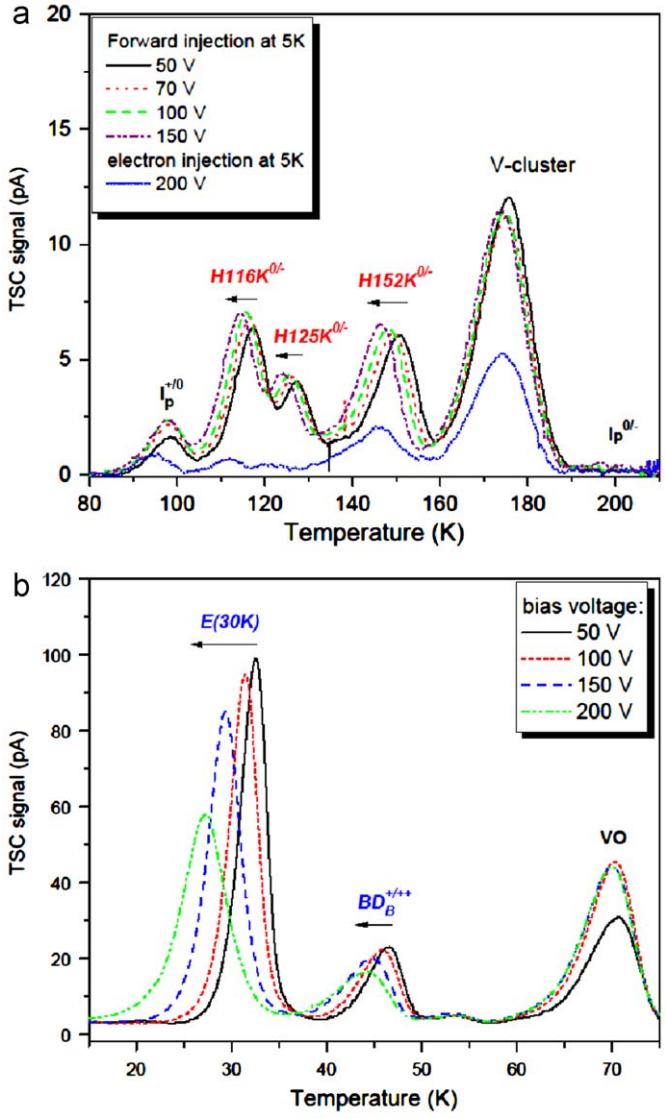

Fig. 7. Poole–Frenkel shift of acceptor and donor peaks with electric field, TSC measurements performed on EPI-DO. (a) Effect of deep hole traps, neutron irradiation with $\Phi_{eq}=5\times10^{13}\,cm^{-2}$, isochronal annealing step at 300 °C (see Fig. 10 (a)); (b) Effect of donor peaks, proton irradiation with $\Phi_{eq}=2.3\times10^{14}\,cm^{-2}$, measured after isothermal annealing for 11,460 min at 80 °C.

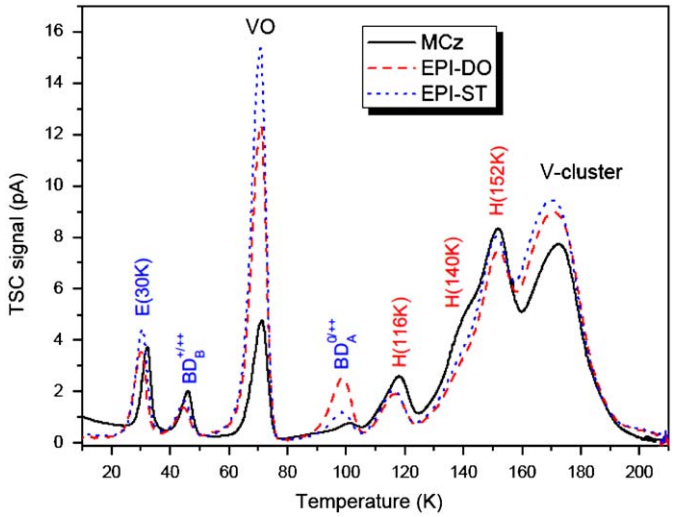

Fig. 8. Comparison of TSC spectra measured on MCz, EPI-DO and EPI-ST diodes after neutron irradiation with $\Phi_{eq}=5\times10^{13}\,cm^{-2}$ after isothermal annealing for 16,980 min at 80 °C.

with those from *C–V* measurements at RT. For a complete evaluation of the effective doping concentration at the different annealing stages in addition to the cluster-related deep hole centers and the *E*(30 K) donor also the contribution from the well-known BDs are taken into account. Another contribution, which could not be extracted from our TSC measurements, was the removal of the P-dopant donors via formation of the E-center (Vacancy–Phosphorus complex). It was added here as a constant contribution not depending on annealing effects. The comparison between the predictions for EPI-DO, EPI-ST and MCz diodes as extracted from the defect analysis and the macroscopic findings are displayed in Figs. 9a, b and c for neutron and Fig. 10 for proton damage. Especially for the neutron irradiation of the EPI-diodes, where the E-center concentration could be reliably extracted macroscopically using the "Hamburg model" (see, e.g. [17,18]), the agreement between prediction and results for the annealing effects is surprisingly good. It should be noted that the MCz diode with its much lower initial doping concentration of only $4.9\times10^{12}\,cm^{-3}$ undergoes type inversion during annealing (around 1000 min at 80 °C), which is very well represented by the microscopic results. Indeed around this annealing time the effective negative space charge given by the net defect concentration equals the initial doping concentration. For the proton irradiation case the large contribution of the *E*(30 K) formation is clearly seen, increasing only during the first 20 min at 80 °C and remaining at a constant level thereafter (see Fig. 10).

In addition to the isothermal annealing so far discussed, predictions from the defect analysis were also demonstrated for isochronal annealing up to 300 °C. An example is given in Figs. 11a and b for a neutron-irradiated EPI-DO diode. It is worth noting that the vacancy cluster (containing the V_2 center and other probably higher-order vacancy complexes) is appreciably narrowing down at higher temperatures, partly due to the annealing of E4, E5 and E6 as also seen in the DLTS study discussed below. The concentrations of the deep hole centers H(116 K) and H(125 K) (the latter not visible in the isothermal annealing studies performed at 80 °C) are steadily increasing, while those for H(140 K) and H(152 K) start to anneal out after reaching a maximum for an annealing temperature around 200 °C. Details of this temperature dependence may be of considerable value for understanding the nature of these defects. The *E*(30 K) donor concentration reaches a maximum after annealing at 240 °C and drops down rapidly at higher annealing temperatures. This and the steady increase in the BD_B strength, transforming into the normal thermal donor, will also have an impact above 200 °C. Finally the concentration of the E-center (donor removal), annealing out above 150 °C, could not be measured in this study as well as other defect transformations (e.g. of di-vacancy in the *X* center for temperatures above 200 °C) which might influence the ΔN_{eff} at room temperature. However, despite all these uncertainties, one can observe that the main temperature dependence for ΔN_{eff} (from *C–V*) is well described by the total concentration of the deep hole traps, as displayed in Fig. 11b. Denoted as acceptors here are only the deep hole traps *H*(116 K), *H*(125 K), *H*(140 K) and *H*(152 K) and as donors are the E(30 K), BD and TDD.

5.5. Striking difference between neutron and proton irradiation

The most obvious difference between neutron and proton irradiation is given by the introduction rate of donors. While the

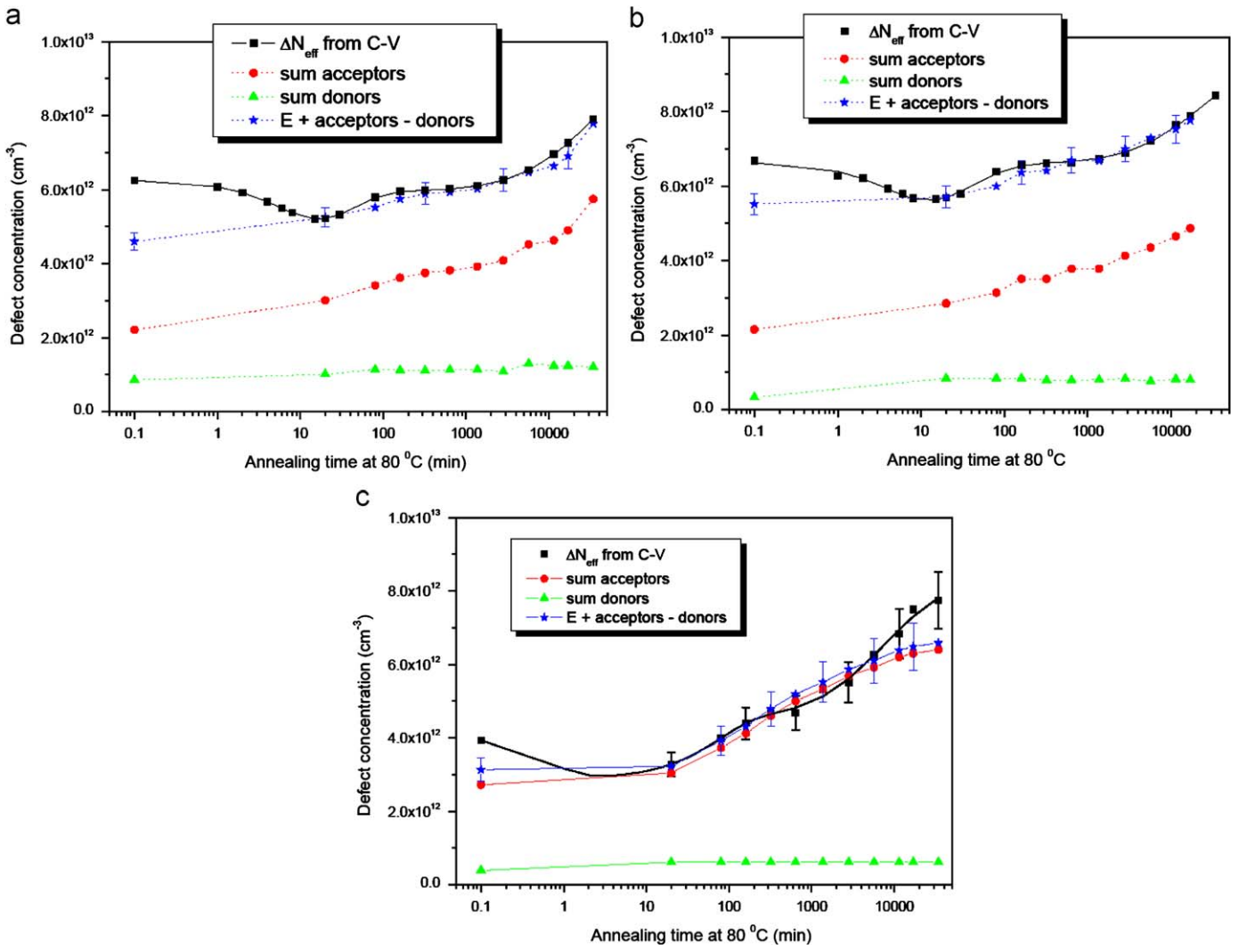

Fig. 9. Comparison of the measured and calculated change of the irradiation-induced effective space charge concentration after neutron irradiation with $\Phi_{eq}=5\times10^{13}\,\mathrm{cm}^{-2}$ at 80 °C annealing (see text). (a) EPI-DO; (b) EPI-ST; (c) MCz.

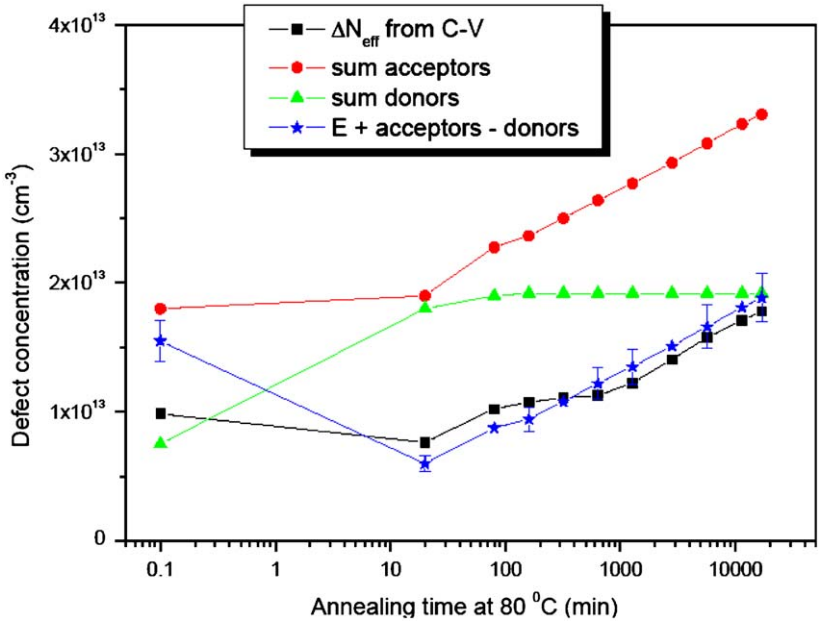

Fig. 10. Same as in Fig. 9 but for an EPI-DO diode irradiated by 23 GeV protons with $\Phi_{eq}=2.3\times10^{14}\,\mathrm{cm}^{-2}$.

BD generation rates are quite similar for neutron and proton induced damage ($1.6\times10^{-2}\,cm^{-1}$ and $2\times10^{-2}\,cm^{-1}$), those for the E(30 K) center are largely different ($9\times10^{-3}\,cm^{-1}$ for n- versus $6\times10^{-2}\,cm^{-1}$ for p-irradiation). For short annealing times around the minimum of ΔN_{eff} (so-called "stable damage component" in the Hamburg model) the large $E(30\,K)$ concentration after proton irradiation leads to an over-compensation of the deep hole centers and thus, in contrast to neutron damage, the effective doping remains positive, increasing with fluence (Fig. 12).

5.6. Correlation with reverse current

As mentioned in Section 2 the reverse current is much more sensitive already to small fluence levels and thus related defects can be well studied with DLTS measurements. For hadron irradiation the responsible defects are likely cluster dominated and thus we concentrated our measurements on mid-gap defect levels. Contrary to the isothermal annealing studies of N_{eff} at 80 °C described before, we present here results of isochronal annealing experiments performed with a neutron-irradiated MCz diode ($\Phi_{eq}=3\times10^{11}\,cm^{-2}$) in the temperature range 20–200 °C. One example of the obtained DLTS spectra before and after annealing at different temperatures is shown in Fig. 13a. The broad DLTS peak centered at around 200 K is composed of at least 4 cluster-related electron traps, which are labeled E4, E5, E6 and $V_2^{-/0}$. While the levels E4 and E5 [65,69–71] decrease even at moderate temperatures and vanish after annealing at 100 °C for 30 min, the defect complex E6 (referred to as E205a in Ref. [72]) is more stable and anneals out in the temperature range100–200 °C. The concentrations of the cluster-related defects cannot be obtained directly from the DLTS spectra, due to their overlap with the singly charged state of the di-vacancy. Therefore, difference in spectra during the annealing process were analyzed, i.e. the difference between the spectrum before annealing and those recorded after each annealing step. Fig. 13b

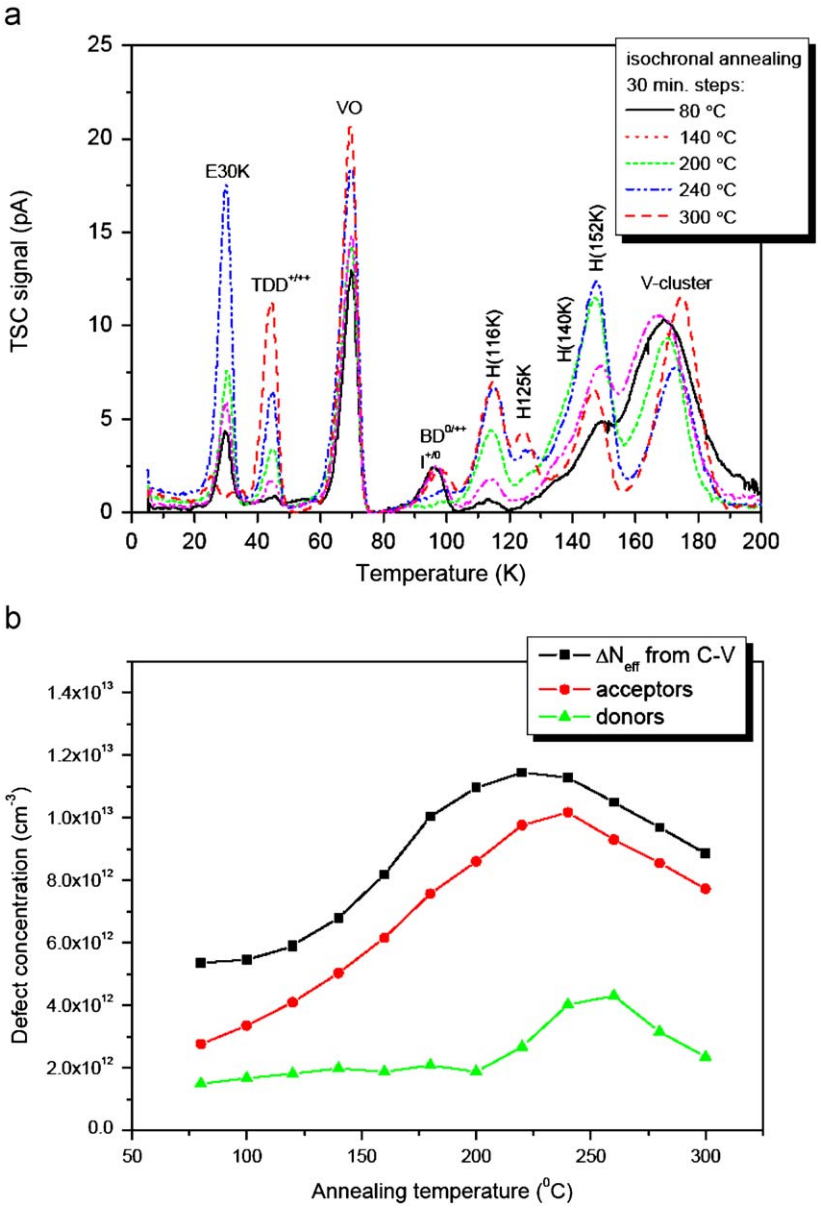

Fig. 11. Measurements taken at isochronal annealing between 80 and 300 °C on an EPI-DO diode, after neutron irradiation with $\Phi_{eq}=5\times10^{13}\,cm^{-2}$. (a) Examples of TSC spectra at several temperature steps; (b) change of effective space charge concentration, extracted from *C–V* curves, in comparison to defect concentrations extracted from TSC results.

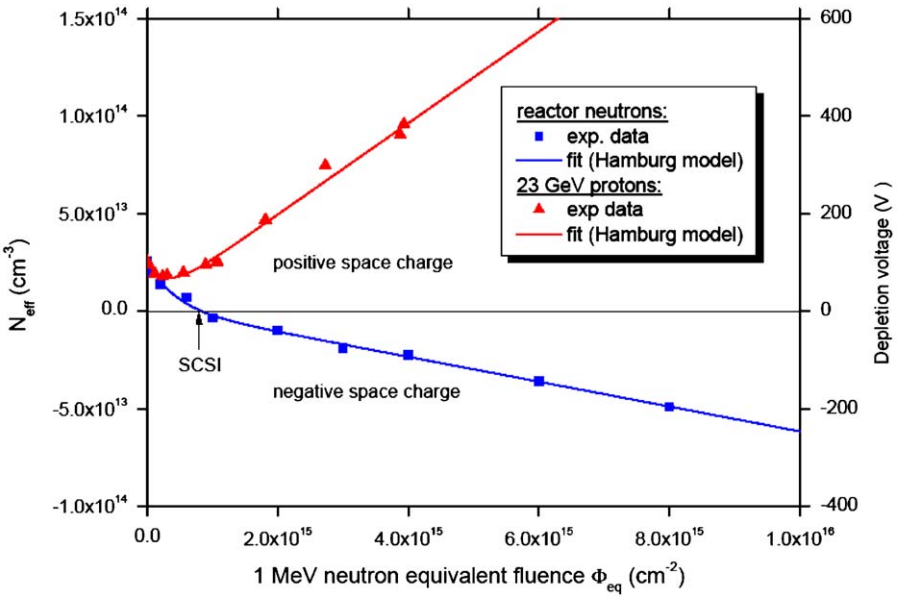

Fig. 12. Effective space charge concentration, extracted from *C–V* measurements in EPI-DO diodes as function of fluence for reactor neutron and 23 GeV proton irradiation.

shows the change of the reverse current versus the corresponding change of the defect concentration, taken during the isochronal annealing in 20 °C steps with an annealing time of 30 min each. The defects, which were taken into account are the levels E5 and E6. Also the change of the reverse current refers to the difference between the value before annealing and those obtained after each annealing step. It is clearly seen, that the leakage current and the cluster-related defect concentration are correlated. The dashed line indicates a possible linear correlation.

The formation of all these cluster-related defects is not affected by the oxygen content of the material or the silicon growth process suggesting that they are complexes of multi-vacancies and/or multi-interstitials located inside extended disordered regions. Presently there are no decisive experiments which would clarify the identity of the observed cluster-related defects *H*(116 K), *H*(140 K), *H*(152 K), *E*(30 K), E4, E5 and E6. Correlated fundamental studies with structure sensitive methods (e.g. Infrared Absorption and EPR) have to be performed in the future.

6. Studies after electron irradiation

As discussed in Section 2, irradiations with several MeV electrons should already result in the generation of cluster-related defects as seen after hadron irradiations but depending on the energy the ratio between cluster and point defects will vary. In order to test this assumption we reinvestigated some TSC measurements after 6 and 15 MeV electron irradiation. The spectra as seen directly after irradiation (no annealing performed in this case) are shown in Fig. 14a (6 MeV electron irradiation with 4 different fluences) and Fig. 14b (comparison between 6 and 15 MeV).

The spectra are very similar to those observed after hadron irradiations, However the following remarks should be taken into account. The peak labeled E(30 K) is surely the same donor defect as seen in neutron and much more pronounced in proton irradiation (see Figs. 6a and b). It is therefore most likely produced by small PKA energies as expected from Coulomb interaction of charged hadrons or electrons. It is however not seen after γ-irradiation and could tentatively be attributed to the tri-interstitial (minimum threshold energy 75 eV) as observed in photoluminescence measurements [46]. For the electron irradiations only oxygen lean float-zone diodes (STFZ) have been used and therefore the generation of the BD-defect, as visible in the hadron-irradiated oxygen-rich EPI-diodes, is very unlikely. Instead at 98 K a large peak, rapidly growing with increasing fluence is detected and identified as the +/0 level of the I_p defect (compare with Fig. 2a). Also the 0/– level of I_p (at about 200 K) is visible but possibly due to the implications by the deep cluster defects the occupation probability is reduced. At the large temperature range the deep hole traps as discovered in hadron irradiations are clearly visible here too. Comparing the spectra for 6 and 15 MeV electron irradiation (Fig. 14b) it is clearly seen that the concentration of the deep hole traps (*H*(116 K), *H*(140 K), *H*(152 K)) is increasing with increase in energy thus supporting the expectation that the cluster formation should largely increase from 6 to 15 MeV. On the other hand the *E*(30 K) concentration is even slightly decreasing, hence again supporting the conclusion that it is not cluster related but an isolated point defect. Finally in Fig. 15 the extracted defect concentrations for 6 MeV irradiations are plotted as function of electron fluence. The concentrations for *E*(30 K) and the deep hole traps are proportional to the fluence whereas for the 98 K defect the fit function is doubtless quadratic (compare with Fig. 2b after γ-irradiation), confirming again that the I_p defect, i.e. the V_2O center, is generated via a second-order process.

7. Summary

Future colliding beam experiments at, e.g. the S-LHC with hadron fluences up to several 10^{16} cm^{-2} in the innermost layers of the tracking area will place an unprecedented challenge for the radiation tolerance of silicon sensors not yet met by present day devices. Improvements have been shown to be possible by certain modifications of the silicon material, process technology and operational conditions. But success oriented endeavors need to be based on a detailed understanding of the damage effects in the silicon bulk and their implications on detector performance.

For the first time a close correlation between the findings by defect spectroscopy and the resulting damage effects in the

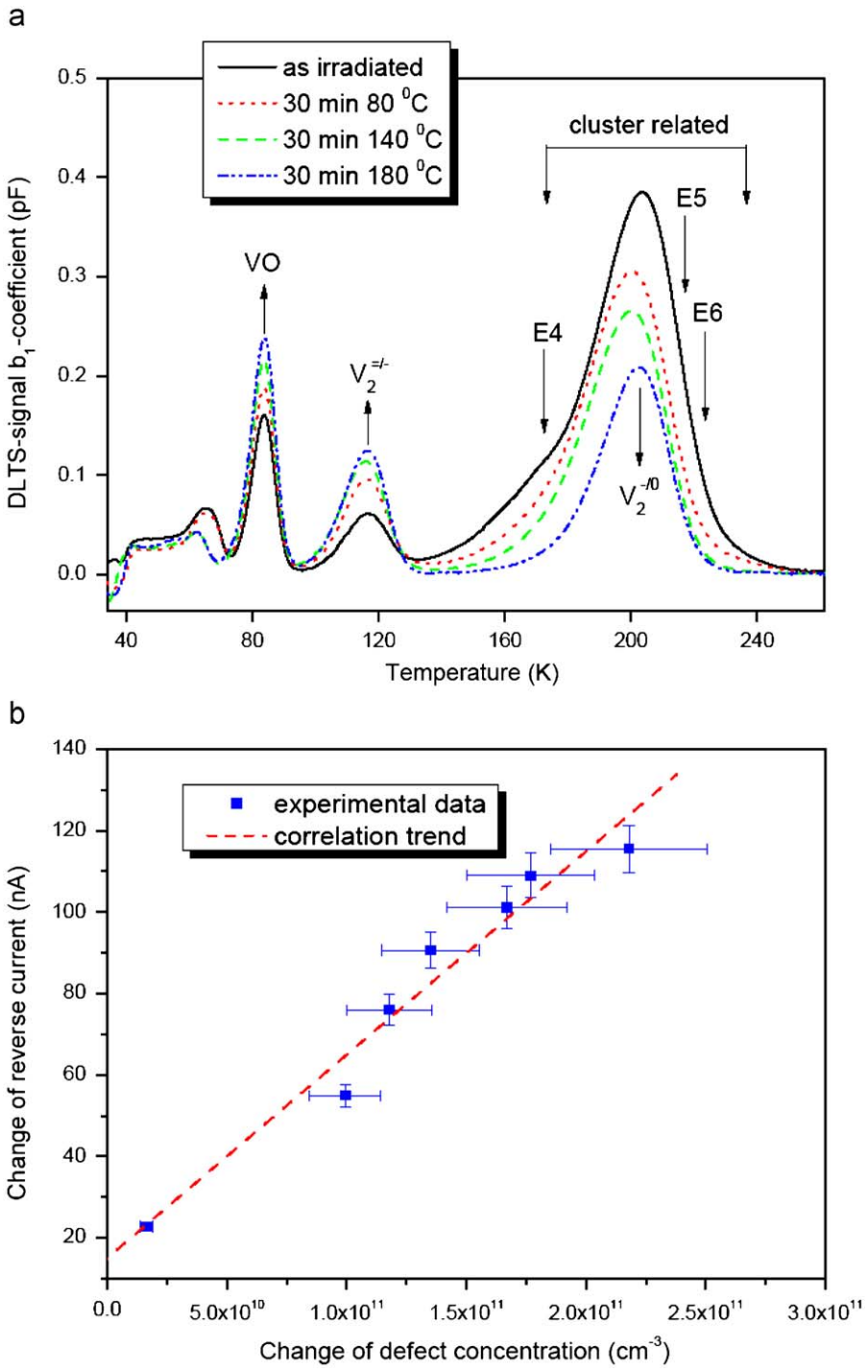

Fig. 13. (a) DLTS spectra measured on a MCz diode after neutron irradiation with $\Phi_{eq}=3\times10^{11}\,cm^{-2}$, examples of isochronal annealing steps between 20 and 200 °C; (b) correlation between the changes of defect concentration as measured by DLTS and the reverse current at full depletion as extracted from *I–V* characteristics.

detector properties are demonstrated in a comprehensive study. A first breakthrough in this respect was achieved by detailed investigations of the damage effects after intense γ-irradiation, where only point defect generation is possible. Both the change of the space charge concentration (depletion voltage) and the increase in the reverse current are now completely understood in terms of radiation-induced defects. Experiments have been extended up to 5 MGy using standard and oxygen-enriched FZ diodes. While the deep acceptor I_p with a level close to mid-gap controls both the increase in negative space charge and the generation current, the shallow bistable donor BD is responsible for increase in positive space charge. The introduction rate of both defects depends on the oxygen content of the material. Especially the quadratic dose dependence of the I_p-defect concentration, indicating a second-order process, the strong reduction of its introduction rate in oxygen-rich material and the thermal stability have lead to a possible assignment with the long searched for V_2O center. In oxygen-enriched material the generation of the BD prevails and overcompensates the I_p center such that the diodes stay at positive space charge up to 5 MGy.

In recent years it was also possible to obtain very promising results for the much more complicated case of hadron-induced

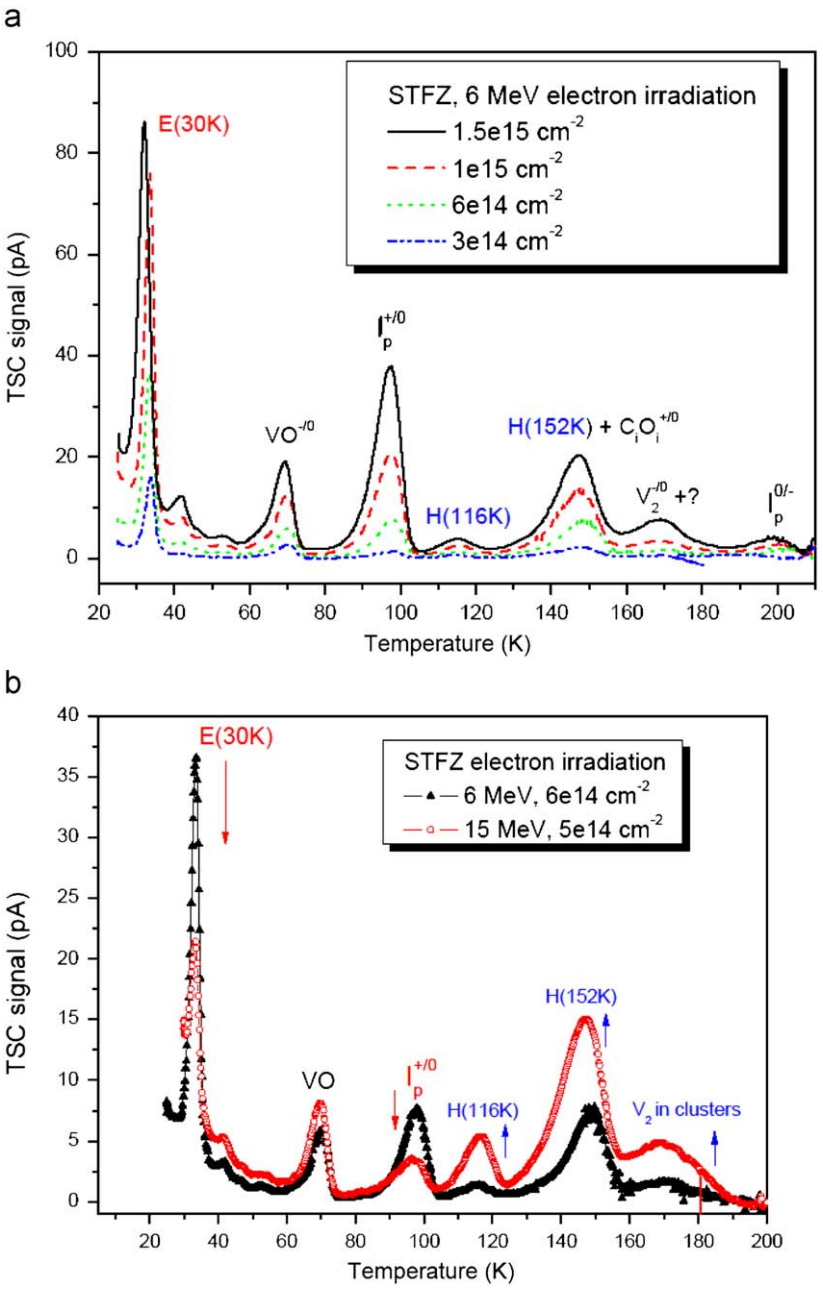

Fig. 14. (a) TSC spectra measured on STFZ diodes irradiated by 6 MeV electrons with 4 different fluences, measurements performed with forward injection at 25 K before annealing; (b) comparison of TSC spectra as measured in STFZ diodes irradiated by 6 and 15 MeV electrons.

damage. Experiments have been performed using standard and oxygen-enriched EPI as well as MCz diodes. It is shown that in addition to point defects a diversity of extended defects as densely packed conglomerates (clusters) of vacancies or interstitials play a dominant role leading to the observed change in the space charge concentration and hence depletion voltage. The three defect centers $H(116\,K)$, $H(140\,K)$ and $H(152\,K)$ are hole traps and show the well-known Poole–Frenkel effect, demonstrating that they are acceptors with levels in the lower half of the band gap. Hence they contribute fully with negative space charge to the effective doping concentration at room temperature. On the other hand two shallow donors ($E(30\,K)$ and BD) are positively charged at room temperature and therefore partly compensate the negative space charge induced by the acceptors. In contrast to the deep acceptors the $E(30\,K)$ donor generation after proton irradiation is strongly enhanced with respect to neutron damage, thus explaining that for proton irradiation the effective space charge remains positive while after neutron damage type inversion is observed. The $E(30\,K)$ defect was only detected after hadron and electron irradiation and is likely related to multi-interstitials. In contrast to γ-irradiation the formation of the BD and I_p defects play a comparatively minor role in hadron irradiation.

Finally we like to emphasize that in addition to previous investigations of γ-irradiation the damage effects after hadron irradiation, especially the annealing behavior, as seen at "macroscopic scale", can now be understood by the "microscopically" investigated kinetics of the responsible defects. The cluster-related defects detected so far and presented in this work seem to be independent of the material. The results toward a complete understanding are very promising. They are regarded to be an excellent basis for further dedicated defect engineering. The present investigations will be extended to larger fluences and

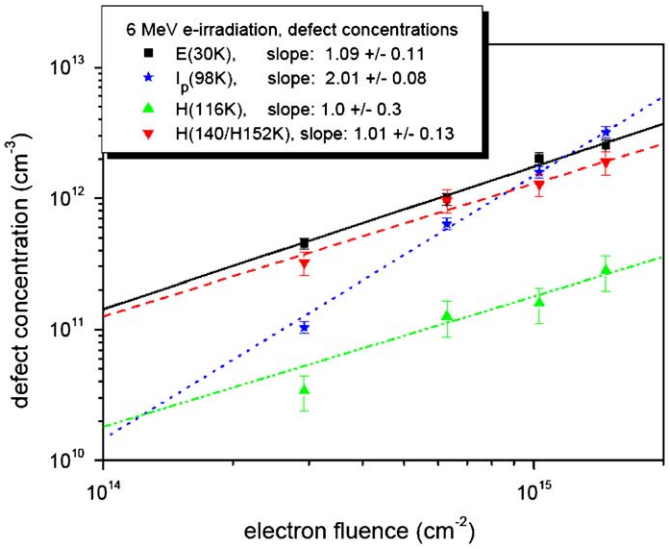

Fig. 15. Dependence of defect concentrations on 6 MeV electron fluence, representation in log–log scale, dotted lines show fits through data, slope of 1 indicates linear dependence for E(30 K) and the deep hole traps H(116 K), H(140 K)+H(152 K), while the I_p defect at 98 K shows a purely quadratic dependence as expected (see Fig. 2b).

include a systematic comparison between neutron and proton damage. An improvement in the radiation hardness is possible only by compensation of the cluster-related acceptors with enhanced donor generation, as achieved in oxygen-enriched material, or inhibiting the vacancy cluster effects, possible via hydrogen enrichment. Especially the latter possibility will be pursued by us in the future.

Acknowledgements

This work was carried out in the frame of the CERN-RD50 collaboration and funded partly by the CiS Hamburg Project under Contract no. SSD 0517/03/05, the BMBF under Contract no. 05HC6GU1 and by the Romanian Ministry of Education and Research under the Core Program, contract 45N/2009. We gratefully thank E. Nossarzewska at ITME, Warsaw, for her professional work in preparing the EPI-diodes and performing the spreading resistance measurements. Likewise the help of A. Barcz at ITE, Warsaw, was invaluable in doing the SIMS measurements. All diode processing had been done by CiS, Erfurt, managed by R. Röder, and we like to express our many thanks for the very successful cooperation. Many thanks are also especially due to G. Kramberger for the neutron irradiation at the TRIGA reactor at JSI Ljubljana, Z. Li for carrying out the γ-irradiation at BNL and M. Glaser for the proton irradiation at the CERN PS facility and B.G. Svensson for providing the electron irradiations at Stockholm. One of us, I. Pintilie, is deeply indebted to R. Klanner, University of Hamburg, for support during several guest stays and numerous discussions. She also likes especially to thank the Humboldt foundation for providing a Humboldt fellowship to her for conducting main parts of this work.

References

[1] F. Gianotti, M.L. Mangano, T. Virdee, Physics potential and experimental challenges of the LHC luminosity upgrade, CERN TH/2002-078, 2002.
[2] G. Grübel, Comptes Rendus Physique 9 (5–6) (2008) 668.
[3] M.A. Vos, Nucl. Instr. and Meth. Phys. Res. A 596-1 (2008) 291.
[4] M. Moll, On behalf of the CERN-RD50 collaboration, Nucl. Instr. and Meth. Phys. Res. A 565 (2006) 202.
[5] G. Kramberger, On behalf of the CERN-RD50 collaboration, recent results from CERN RD50 collaboration, Nucl. Instr. and Meth. Phys. Res. A 583 (2007) 49.
[6] E. Fretwurst, On behalf of the CERN-RD50 collaboration, Nucl. Instr. and Meth. Phys. Res. A 552 (2005) 7.
[7] G. Lindström, E. Fretwurst, F. Hönniger, G. Kramberger, M. Möller-Ivens, I. Pintilie, A. Schramm, Nucl. Instr. and Meth. Phys. Res. A 556 (2006) 441.
[8] E. Fretwurst, G. Lindström, J. Stahl, I. Pintilie, Z. Li, J. Kierstead, E. Verbitskaya, R. Röder, Nucl. Instr. and Meth. Phys. Res. A 514 (2003) 1.
[9] E. Tuovinen, J. Härkönen, P. Luukka, E. Tuominen, E. Verbitskaya, V. Eremin, I. Ilyashenko, A. Pirojenko, I. Riihimäki, A. Virtanen, K. Leinonen, Nucl. Instr. and Meth. Phys. Res. A 568 (2006) 83.
[10] E. Fretwurst, L. Andricek, F. Hönniger, G. Kramberger, G. Lindström, G. Lutz, M. Reiche, R.H. Richter, A. Schramm, Nucl. Instr. and Meth. Phys. Res. A 552 (2005) 124.
[11] J. Härkönen, E. Tuovinen, P. Luukka, E. Tuominen, K. Lassila-Perini, P. Mehtälä, S. Nummela, J. Nysten, A. Zibellini, Z. Li, E. Fretwurst, G. Lindström, J. Stahl, F. Hönniger, V. Eremin, A. Ivanov, E. Verbitskaya, P. Heikkilä, V. Ovchinnikov, M. Yli-Koski, P. Laitinen, A. Pirojenko, I. Riihimäki, A. Virtanen, Nucl. Instr. and Meth. Phys. Res. A 518 (2004) 346.
[12] G. Kramberger, V. Cindro, I. Mandic, M. Mikuž, Nucl. Instr. and Meth. Phys. Res. A 579 (2007) 762.
[13] G. Kramberger, V. Cindro, I. Dolenc, E. Fretwurst, G. Lindström, I. Mandic, M. Mikuž, M. Zavrtanik, Nucl. Instr. and Meth. Phys. Res. A 554 (2005) 212.
[14] V. Khomenkov, D. Bisello, M. Bruzzi, A. Candelori, A. Litovchenko, C. Piemonte, R. Rando, F. Ravotti, N. Zorzi, Nucl. Instr. and Meth. Phys. Res. A 568 (2006) 61.
[15] A. Ruzin, G. Casse, M. Glaser, A. Zanet, F. Lemeilleur, S. Watts, IEEE Trans. Nucl. Sci. NS-46 (5) (1999) 1310.
[16] Z. Li, B. Dezillie, M. Bruzzi, W. Chen, V. Eremin, E. Verbitskaya, P. Weilhammer, Nucl. Instr. and Meth. Phys. Res. A 461 (2001) 126.
[17] G. Lindström, On behalf of the CERN-RD48 Collaboration, Developments for radiation hard silicon detectors by defect engineering-results by the CERN RD48 (ROSE) collaboration, Nucl. Instr. and Meth. Phys. Res. A 465 (2001) 60.
[18] G. Lindström, on behalf of the CERN-RD48 collaboration, radiation hard silicon detectors-developments by the RD48 (ROSE) collaboration, Nucl. Instr. and Meth. Phys. Res. A 466 (2001) 308.
[19] Siltronic AG, 81737 Munich, Germany.
[20] Okmetic Oyj, 01510 Vantaa, Finland.
[21] Institute of Electronic Materials Technology (ITME), 01919 Warsaw, Poland.
[22] G. Lindström, I. Dolenc, E. Fretwurst, F. Hönniger, G. Kramberger, M. Moll, E. Nossarzewska, I. Pintilie, R. Röder, Nucl. Instr. and Meth. Phys. Res. A 568 (2006) 66.
[23] CiS Research Institute for Micro Sensors and Photovoltaics GmbH, 99099, Erfurt, Germany.
[24] A. Barcz, M. Zielinski, E. Nossarzewska, G. Lindström, Appl. Surface Sci. 203–204 (2003) 396; A. Barcz, Institute of Physics PAS, 02-668 Warsaw, Poland, private communication.
[25] E. Nossarzewska, Institute of Electronic Materials Technology (see [21]), private communication.
[26] Z. Li, J. Kierstead, Solid State Gamma-ray Irradiation Facility, Brookhaven National Laboratory BNL, Upton, NY 11973, USA.
[27] B.G. Svensson, Physics Institute, University of Oslo, 0316 Oslo, Norway.
[28] V. Cindro, G. Kramberger, Jozef Stefan Institute, 1111 Ljubljana, Slovenia, TRIGA Reactor: n-Irradiation Facility.
[29] M. Glaser, CERN Division EP-TA1-SD, Geneva, Switzerland, Proton Irradiation Facility Irrad-1.
[30] J.A. van Lint, T.M. Flanagan, R.E. Leadon, J.A. Naber, V.C. Rogers, John Wiley & Sons, 1980.
[31] M. Huhtinen, Nucl. Instr. and Meth. Phys. Res. A 491 (2002) 194.
[32] A. Vasilscu, G. Lindström, M. Huhtinen, private communication 1999, see RD48 Third Status Report, CERN/LHCC 2000-009 (1999), pp. 39–41.
[33] I. Pintilie, L. Pintilie, M. Moll, E. Fretwurst, G. Lindström, Appl. Phys. Lett. 78 (2001) 550.
[34] I. Pintilie, M. Buda, E. Fretwurst, G. Lindström J. Stahl, Nucl. Instr. and Meth. Phys. Res. A 556 (2006) 197.
[35] G.D. Watkins, J.W. Corbett, Phys. Rev. 121 (4) (1961) 1001.
[36] G.D. Watkins, J.W. Corbett, Phys. Rev. 134 (5A) (1964) A1359.
[37] G.D. Watkins, J.W. Corbett, Phys. Rev. 138 (2A) (1965) A543.
[38] S.D. Brotherton, P. Bradley, J. Appl. Phys. 53 (1982) 5720.
[39] L.C. Kimerling, in: N.B. Urli, J.W. Corbett (Eds.), Radiation Effects in Semiconductors 1976, Conference Series No. 31, The Institute of Physics, Bristol, 1977, p. 221.
[40] O.O. Awadelkarim, H. Weman, B.G. Svensson, J.L. Lindström, J. Appl. Phys. 60 (6) (1986) 1974.
[41] B.G. Svensson, B. Mohadjeri, A. Hallén, J.H. Svensson, J.W. Corbett, Phys. Rev. B 43 (1991) 2292.
[42] A. Hallén, N. Keskitalo, F. Masszi, V. Nágl, J. Appl. Phys. 79 (1996) 3906.
[43] M. Moll, H. Feick, E. Fretwurst, G. Lindström, C. Schultze, Nucl. Instr. and Meth. Phys. Res. A 388 (1997) 335.
[44] J. Hermansson, L.I. Murin, T. Hallberg, V.P. Markevich, J.L. Lindström, M. Kleverman, B.G. Svensson, Phys. B: Condens. Matter 302–303 (2001) 188.
[45] E.V. Monakhov, B.S. Avset, A. Hallén, B.G. Svensson, Phys. Rev. B 65 (2002) 233207.
[46] G. Davies, S. Hayama, L. Murin, R. Krause-Rehberg, V. Bondarenko, A. Sengupta, C. Davia, A. Karpenko, Phys. Rev. B 73 (2006) 165202.

[47] P. Bräunlich, in: P. Bräunlich (Ed.), Thermally Stimulated Relaxation in Solids, Springer-Verlag, Berlin, 1979, p. 1 (Chapter 1).
[48] I. Pintilie, E. Fretwurst, G. Lindström, J. Stahl, Nucl. Instr. and Meth. Phys. Res. A 514 (2003) 18.
[49] J.L. Hartke, J. Appl. Phys. 39 (1968) 4871.
[50] I. Pintilie, E. Fretwurst, G. Lindström, J. Stahl, Appl. Phys. Lett. 81 (1) (2002) 165.
[51] I. Pintilie, E. Fretwurst, G. Lindström, J. Stahl, Appl. Phys. Lett. 82 (2003) 2169.
[52] I. Pintilie, E. Fretwurst, G. Kramberger, G. Lindstroem, Z. Li, J. Stahl, Phys. B: Condens. Matter 340–342 (2003) 578.
[53] Y.H. Lee, J.W. Corbett, Phys. Rev. B 13 (6) (1976) 2653.
[54] Y.H. Lee, T.D. Bilash, J.W. Corbett, Radiat. Eff. 29 (1976) 7.
[55] G. Alfieri, E.V. Monakhov, B.S. Avset, B.G. Svensson, Phys. Rev. B 68 (2003) 233202.
[56] M. Mikelsen, E.V. Monakhov, G. Alfieri, B.S. Avset, B.G. Svensson, Phys. Rev. B 72 (2005) 195207.
[57] E. Fretwurst, F. Hönniger, G. Kramberger, G. Lindström, I. Pintilie, R. Röder, Nucl. Instr. and Meth. Phys. Res. A 583-1 (2007) 58.
[58] I. Pintilie, E. Fretwurst, G. Lindström, Appl. Phys. Lett. 92 (2008) 024101.
[59] P. Wagner, J. Hage, Appl. Phys. A 49 (1989) 123.
[60] Y.A.I. Latushko, L.F. Makarenko, V.P. Markevich, L.I. Murin, Phys. Status Solidi (A) 93 (1986) K181.
[61] A. Chantre, Appl. Phys. Lett. 50 (21) (1987) 1500.
[62] P.W. Anderson, Phys. Rev. Lett. 34 (1975) 953.
[63] B.C. MacEvoy, Nucl. Instr. and Meth. Phys. Res. A 388 (1997) 365.
[64] M. Pesola, Y.J. Lee, J. von Boehm, M. Kaukonen, R.M. Nieminen, Phys. Rev. Lett. 84 (23) (2000) 5343.
[65] R.M. Fleming, C.H. Seager, D.V. Lang, P.J. Cooper, E. Bielejec, J.M. Campbell, J. Appl. Phys. 102 (2007) 043711.
[66] R.M. Fleming, C.H. Seager, D.V. Lang, E. Bielejec, J.M. Campbell, J. Appl. Phys. 104 (2008) 083702.
[67] M. Bruzzi, et al., Nucl. Instr. and Meth. Phys. Res. A 552 (2005) 20.
[68] M. Scaringella, D. Menichelli, M. Bruzzi, A. Macchiola, C. Piemonte, N. Zorzi, A. Candelori, V. Eremin, E. Verbitskaya, I. Pintilie, Nucl. Instr. and Meth. Phys. Res. A 570 (2007) 322.
[69] M. Moll, E. Fretwurst, M. Kuhnke, G. Lindström, Nucl. Instr. and Meth. Phys. Res. B 186 (2002) 100.
[70] S.J. Watts, J. Matheson, I.H. Hopkins-Bond, A. Holmes-Siedle, A. Mohammadzadeh, R. Pace, IEEE Trans Nucl. Sci. NS-43 (1996) 2587.
[71] A. Junkes, D. Eckstein, I. Pintilie, L.F. Makarenko, E. Fretwurst, Annealing study of a bistable cluster defect, Nucl. Instr. and Meth. Phys. Res. A. (2009), doi:10.1016/j.nima.2009.08.021.
[72] M. Moll, Radiation Damage in Silicon Particle Detectors—Microscopic Defects and Macroscopic Properties, PhD Thesis, DESYTHESIS-1999-040, 1999.